Prace Naukowe IICh PAN, 17, 59÷79 (2013)

MARZENA IWANISZYN[1], JOANNA ŁOJEWSKA[2], ANDRZEJ KOŁODZIEJ[1]

COMPUTATIONAL FLUID DYNAMICS MODELING OF HEAT TRANSFER AND FLOW RESISTANCE IN SHORT CHANNELS: DETAILED DESCRIPTION

1 - Institute of Chemical Engineering Polish Academy of Sciences, ul. Bałtycka 5, 44-100 Gliwice
2 - Jagiellonian University, Faculty of Chemistry, ul. Ingardena 3, 33-060 Kraków

Effect of the internal geometry of catalytic reactor capillary channels have been studied by means of numerical simulations. ANSYS FLUENT software was applied for carrying the analysis out. The temperature and pressure distribution for different channel lengths and cross-sectional shapes were presented.

Wpływ geometrii wewnętrznej kapilarnych kanałów reaktorów katalitycznych badano za pomocą symulacji komputerowych. Do przeprowadzenia analizy zastosowano oprogramowanie ANSYS FLUENT. Przedstawiono rozkłady temperatur i ciśnienia w kanałach o różnych długościach i kształtach przekrojów poprzecznych.

1. INTRODUCTION

In recent years catalytic combustion has become a fundamental method of abatement of harmful chemicals emitted to the atmosphere. These environmentally hazardous pollutants include, besides others:

- vehicle exhaust gases that consist carbon monoxide (CO), hydrocarbons (HC), nitrogen oxides (NO_x) and particulate matter (PM);
- methane originated from biological sources or ventilation air of mines;
- volatile organic compounds (VOCs), which include hydrocarbons, halogen derivatives, mercaptans, monomers are included in these pollutants.

All emissions are characterized by high toxicity and very low concentrations in gas streams.

Many processes of catalytic combustion are realized in monolithic (ceramic or metallic) reactor, which consists of many parallel channels of different cross-sectional shapes. Generally, the square shape is commonly used (sometimes rectangular, hexagonal, triangular and sinusoidal, as well). The choice of channel cross-sectional shape affects the velocity flow field and thus the flow resistance and heat/mass transfer in the reactor. More details are presented in[1-3].

In narrow capillary channels, the laminar flow commonly occurs. The improvement of mass transfer intensity might be achieved by reduction of the channel length. In the classic long monolith the developed laminar flow mainly occurs and thus parabolic velocity profiles, as well as these of the temperature and concentration, are formed, and transport and hydrodynamic coefficients are small, nearly constant, and they depend mainly on the cross-sectional channel shape and boundary conditions [4]. In the major part of a short channel the developing laminar flow occurs resulting in enhanced mass transfer, but also higher flow resistance (friction factor).

Therefore, single short channels of sinusoidal and triangular shapes are modeled in ANSYS FLUENT to present the channel geometry influence on the heat transfer and flow resistance.

2. MATHEMATICAL MODELLING

The CFD (Computational Fluid Dynamics) code used for this study was ANSYS FLUENT-12 which is fully integrated fluid analysis software of ANSYS Workbench platform. It combines CAD (Computer Aided Design) (modeling and input), complex meshing solutions, fast solution algorithm and post-processing facilities [5,6]. The analysis is carried on to obtain the pressure and temperature for single channels of triangular and sinusoidal cross-section for various operational conditions using air. The mathematical model adopted in this work is based on the following assumptions: the laminar flow is considered, the process is of steady state, radiative and gravitational effects are negligible and the air is considered incompressible.

2.1. GOVERNING EQUATIONS

The governing equations for flow and heat transfer in the single heated channel were solved in the Cartesian coordinate system.

The continuity equation is formulated as follows:

$$\frac{\partial(\rho w_j)}{\partial x_j} = 0 \tag{1}$$

The following equation system represents the momentum equations in Cartesian coordinate system where i, j ϵ {1, 2, 3}:

$$\frac{\partial\left(\rho w_j w_i\right)}{\partial x_j} = -\frac{\partial P}{\partial x_i} + \frac{\partial}{\partial x_j}\left(\eta \frac{\partial w_i}{\partial x_j} + \frac{\partial w_j}{\partial x_i}\right) \tag{2}$$

The following form of the energy equation is solved to calculate the temperature distribution:

$$\frac{\partial\left(\rho c_p w_j T\right)}{\partial x_j} = \lambda \frac{\partial^2 T}{\partial x_j^2} \tag{3}$$

Temperature dependency of different physical properties (λ, c_p, ρ, η) of the working fluid has been considered to improve the accuracy of the calculations. The correlations for calculating the thermo-physical properties of the air expressed as follow:

- density was calculated using incompressible ideal gas law:

$$\rho = \frac{p_{op} M_w}{Rt} \tag{4}$$

- specific heat and thermal conductivity are functions of temperature:

$$c_p = 1009 + 0{,}126t \tag{5}$$

$$\lambda = 0{,}037 + 1{,}67 \cdot 10^{-5} t \tag{6}$$

- dynamic viscosity was calculated using Sutherland's equation:

$$\eta = \frac{17{,}168 \cdot 10^{-5} t^{\frac{3}{2}}}{t + 114} \tag{7}$$

The solid material is kanthal steel with constant properties:

- density: ρ=7150 [kg·m^{-3}]
- specific heat: c_p=460 [J·kg^{-1}·K^{-1}]
- thermal conductivity: λ=13 [W·m^{-1}·K^{-1}]

Besides specifying the basic set of conservation equations and characteristics of the flow, the boundary conditions must be defined for inlet, outlet and channel wall to solve the model equations. Temperature and velocity are known parameters for the reactor inlet. Constant heat flux is assumed parameter, constant along channel wall. The pressure outlet boundary condition was assumed for the reactor outlet, i. e., the overpressure for the reactor outlet was assumed to be zero.

Conservation equations for the mass, momentum and energy equations along with the boundary conditions for the domain were solved using finite volume method.

2.2. MODEL AND MESH GENERATION

The CAD models of single channels of triangular and sinusoidal cross-section used in the present analysis are shown in Fig. 1. The geometric dimensions (base, height, length and wall thickness) are gathered in Table 1. The control regions before and behind the channel were introduced. In the inlet control region, as well as at the channel inlet, velocity and temperature profiles were assumed uniform. The velocity and temperature profiles are forming during flow through the channel (Fig. 2).

Table 1. Geometric dimensions of channels
Tabela 1. Wymiary geometryczne kanałów

Channel	Length [mm]	Base [mm]	High [mm]	Wall thickness of channel base [mm]	Wall thickness of channel arms [mm]
triangle	5	5.5	4.5	0.1	0.05
	15				
sine	5	4	2.15		
	15				

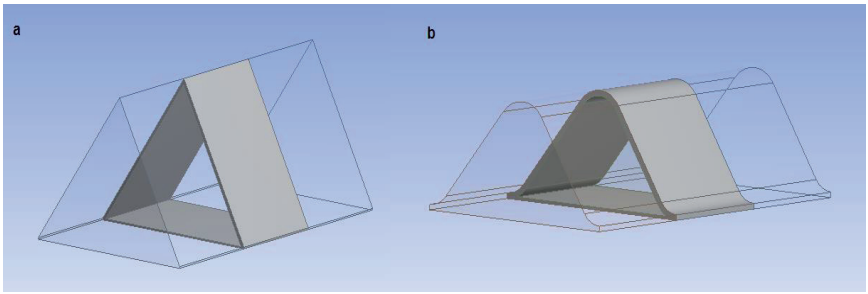

Fig. 1. 3D geometry: a – triangular channel L=5 mm; b – sinusoidal channel L=5 mm
Rys. 1. Geometria trójwymiarowa (3D): a – kanału trójkątnego L=5 mm; b – kanału sinusoidalnego L=5 mm

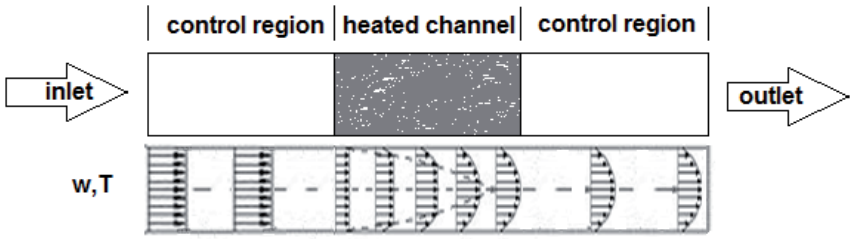

Fig. 2. The formation of velocity and temperature profiles during computational simulations
Rys. 2. Formowanie się profili prędkości i temperatury podczas symulacji komputerowych

ANSYS FLUENT uses an element-based finite volume method, which first involves discretizing the spatial domain using a mesh. The mesh is used to construct finite volumes, which are used to conserve relevant quantities such as mass, momentum, and energy. In this work the grid was generated using a multi-block scheme and is presented in Fig. 3.

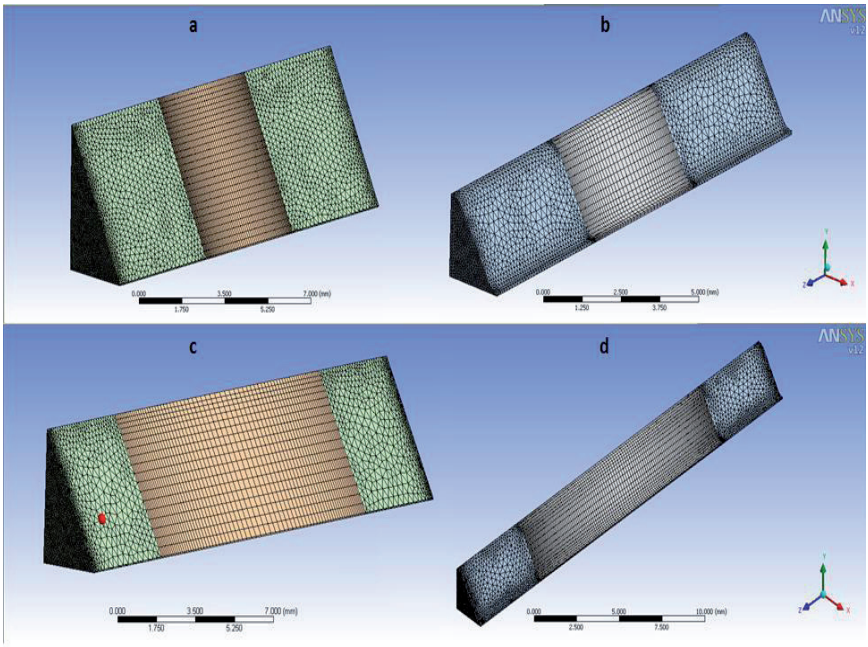

Fig. 3. Mesh: a – triangular channel L=5 mm; b – sinusoidal channel L=5 mm; c – triangular channel L=15 mm; d – sinusoidal channel L=15 mm
Rys. 3. Siatka obliczeniowa: a – kanału trójkątnego L=5 mm; b – kanału sinusoidalnego L=5 mm; c – kanału trójkątnego L=15 mm; d – kanału sinusoidalnego L=15 mm

3. RESULTS AND DISCUSSION

The CFD calculations were performed for the range of flow velocities presented in Table 2. In the subsequent figures, the graphical representations of the pressure and temperature field are done for the maximal velocities from the applied ranges.

Table 2. Structures parameters applied in graphical presentations of numerical calculations
Tabela 2. Parametry struktur stosowane w graficznym przedstawieniu wyników obliczeń numerycznych

structure	L [mm]	w [m s^{-1}] range	t [°C] range	Re range
triangular	5	0.155 – 18.496	26.0 – 66.0	25.514 – 2843.355
	15	0.152 – 18.268	20.3 – 58.2	25.851 – 2878.174
sinusoidal	5	0.153 – 18.359	27.3 – 76.7	13.921 – 1538.378
	15	0.151 – 18.931	25.9 – 80.7	13.408 – 1477.616

3.1. HEAT TRANSFER

The temperature distribution of the air flow and the heated channel wall in selected channel cross-sectional areas are shown in Fig. 4 – 7 (control sections are marked T1 – T3). Section T1 – T2 corresponds to the physically existing channel under the test. Longitudinal local air temperature distributions, presented in the figures, provide the temperature distribution on the plane of the vertical axis of the cross section of the channel.

The air temperature is constant before the channel inlet and corresponds to an initial temperature introduced to the program. During the flow through a heated channel the air temperature rises rapidly in the channel region in close contact with the heated wall. Beyond the channel outlet, the temperature starts to become even as a result of mixing of the fluid. However, achieving mixing fluid temperature requires relatively long distance from the channel outlet.

The velocity profile is uniform (constant) before the inlet to the channel, throughout its cross section. The flat velocity profile is assumed at the channel inlet. The velocity profile is formed during the flow through the channel formed from. After reaching the channel outlet, velocity profile does not change. The model assumes that there is still virtual, not heated channel wall that keeps the velocity profile formed.

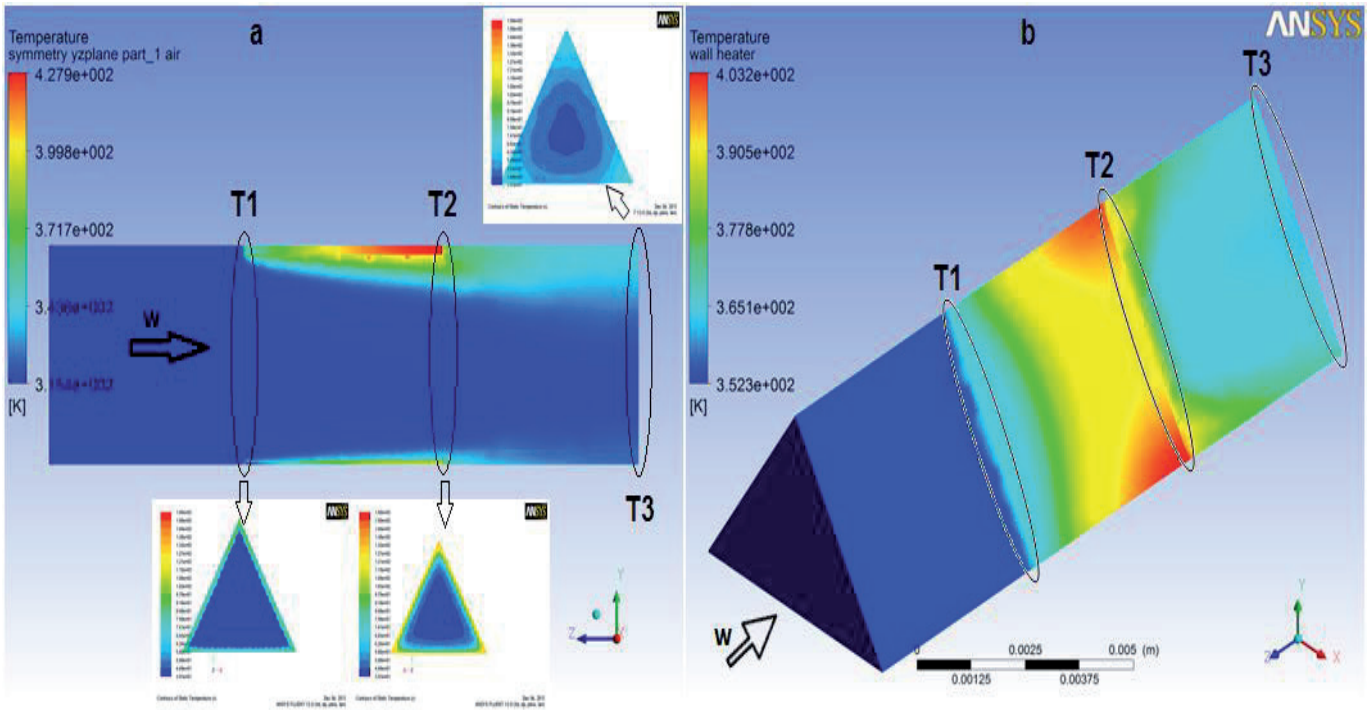

Fig. 4. Temperature distribution in triangular channel (L=5 mm; w=16.507 $m \cdot s^{-1}$; t=42.3 °C; q=24503.570 $W \cdot m^{-2}$): a – in air stream; b – on heated wall

Rys. 4. Rozkład temperatur w kanale trójkątnym (L=5 mm; w=16.507 $m \cdot s^{-1}$; t=42.3 °C; q=24503.570 $W \cdot m^{-2}$): a – w strumieniu powietrza; b – na ogrzewanej ścianie

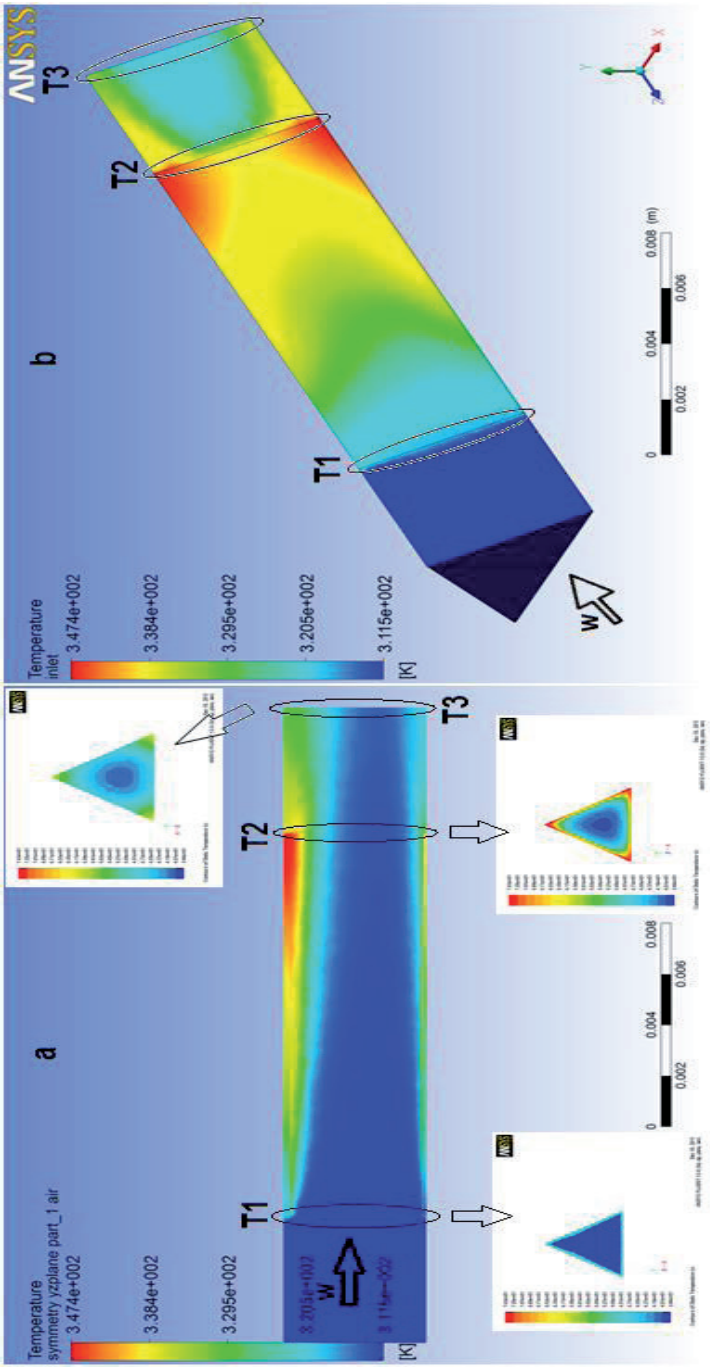

Fig. 5. Temperature distribution in triangular channel (L=15 mm; w=16.231 m·s^{-1}; t=38.9 °C; q=7058.218 W·m^{-2}): a – in air stream; b – on heated wall

Rys. 5. Rozkład temperatur w kanale trójkątnym (L=15 mm; w=16.231 m·s^{-1}; t=38.9 °C; q=7058.218 W·m^{-2}): a – w strumieniu powietrza; b – na ogrzewanej ścianie

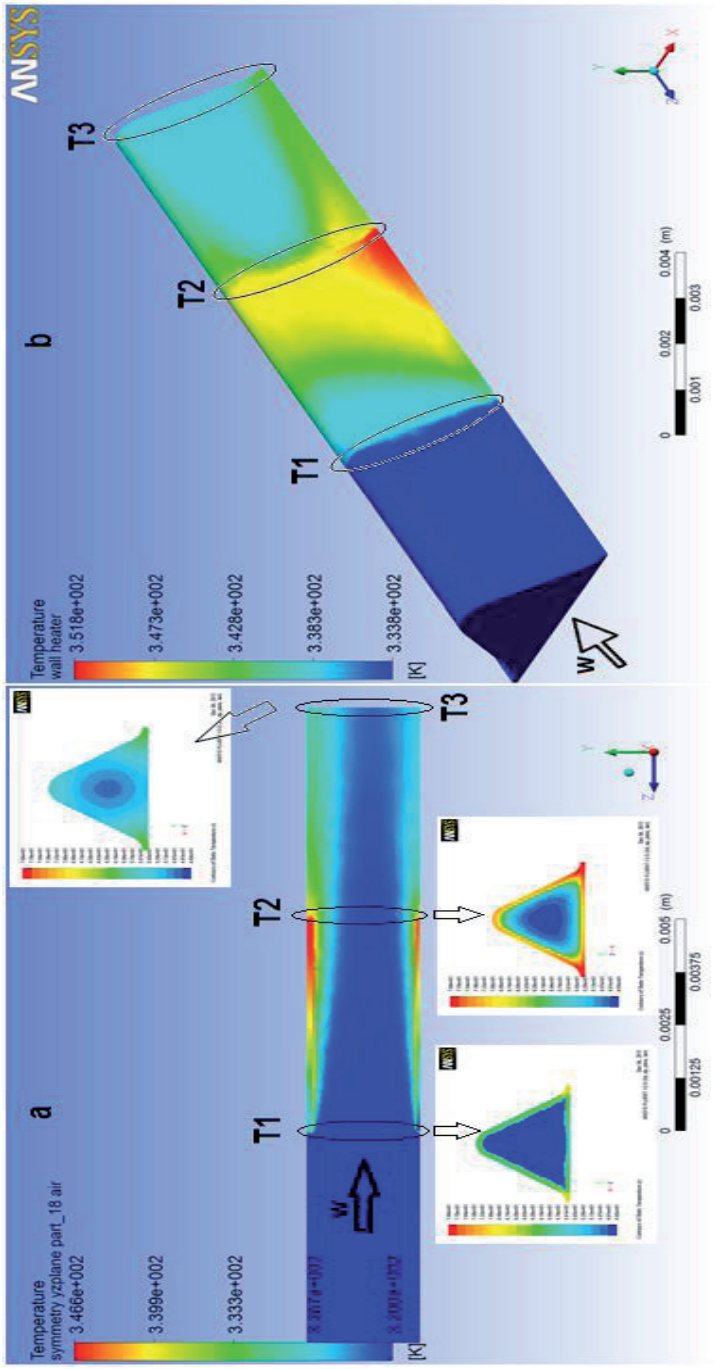

Fig. 6. Temperature distribution in sinusoidal channel (L=5 mm; w=16.595 m·s^{-1}; t=46.9 °C; q=9466.676 W·m^{-2}): a – in air stream; b – on heated wall

Rys. 6. Rozkład temperatur w kanale sinusoidalnym (L=5 mm; w=16.595 m·s^{-1}; t=46.9 °C; q=9466.676 W·m^{-2}): a – w strumieniu powietrza; b – na ogrzewanej ścianie

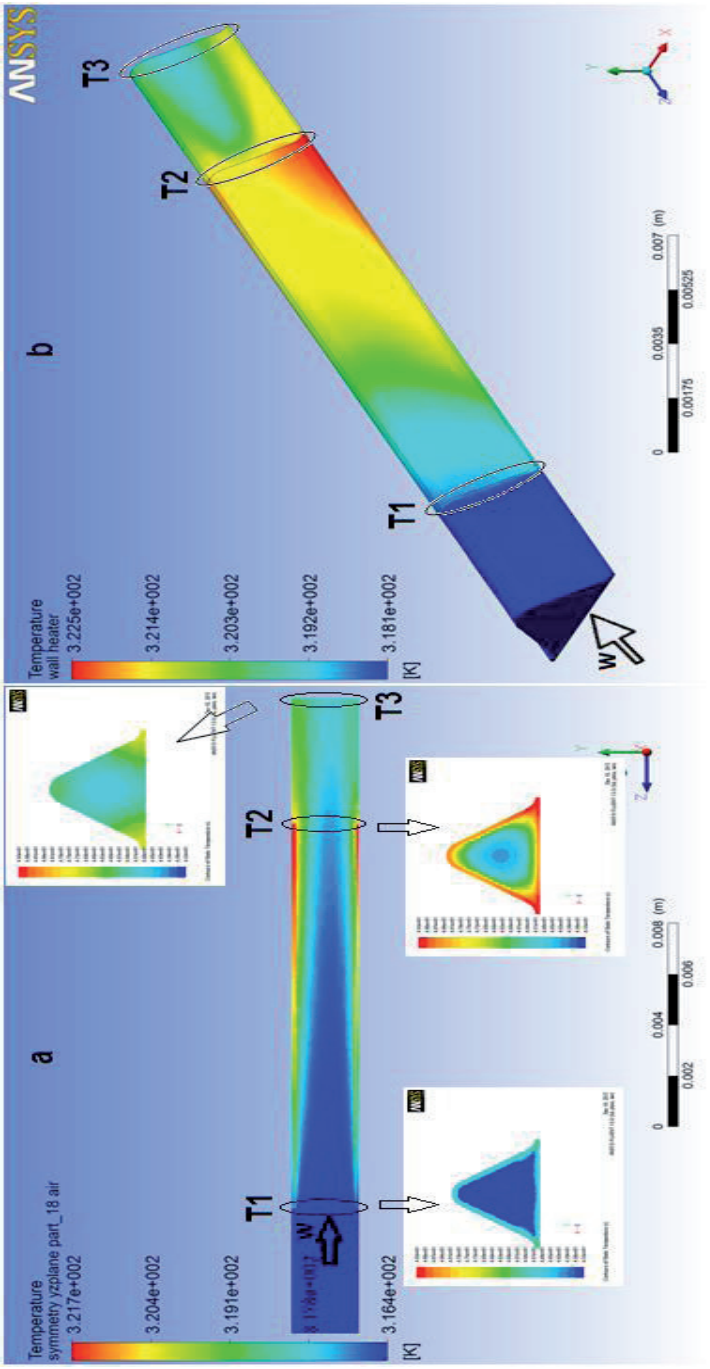

Fig. 7. Temperature distribution in sinusoidal channel (L=15 mm; w=15.604 m·s^{-1}; t=43.3 °C; q=1116.378 W·m^{-2}): a – in air stream; b – on heated wall

Rys. 7. Rozkład temperatur w kanale sinusoidalnym (L=15 mm; w=15.604 m·s^{-1}; t=43.3 °C; q=1116.378 W·m^{-2}): a – w strumieniu powietrza; b – na ogrzewanej ścianie

A comparison sites designated as T2 and T3 in Fig. 4a – 7a shows that the largest temperature gradient appears near to the channel wall in the middle of the triangular/sinusoidal side. The temperature of the air flow is highest within the structures vertices (curvatures). Furthermore, the air flow in sinusoidal channel is heated to a higher temperature, which is the result of approximately two times higher the surface area of the sinusoidal structures compared with the triangular structures. The channel length seriously affects the heat transfer as well. The intensity of heat transfer is larger in the shorter channel as well as in the entrance section of a longer channel. It is necessary to overcome the flowing air stream at a distance from the channel outlet due to the laminar nature of the flow to achieve the temperature equalization (mixing) in the channel cross section (said virtual wall is not heated by the physical channel outlet).

In order to calculate the heat transfer coefficients, thus Nusselt numbers, the average temperature of air stream at the channel inlet and outlet are taken into account (places marked as T1 and T2 in Fig. 4a – 7a). The average temperature at the outlet was calculated as the mixing cup temperature T_m defined as:

$$T_m = \frac{1}{A_c w_m} \int_{A_c} wTdA_c \tag{8}$$

The heat transfer coefficients, average over all the channel walls surface area, as a function of fluid velocity for different channels are presented in Fig. 8. The best result was achieved for triangle channel of 5 mm length. The sine channels lie between triangle channels. However, for high fluid velocities, the sine channels lie close to triangular one, 15 mm long.

Additionally, Fig. 9 – 10 present the temperature distributions in different cross-sectional areas of the channel. Black line shows the wall area, while the red line - the core stream. The place, where the lines meet, indicates the mixing-cup temperature.

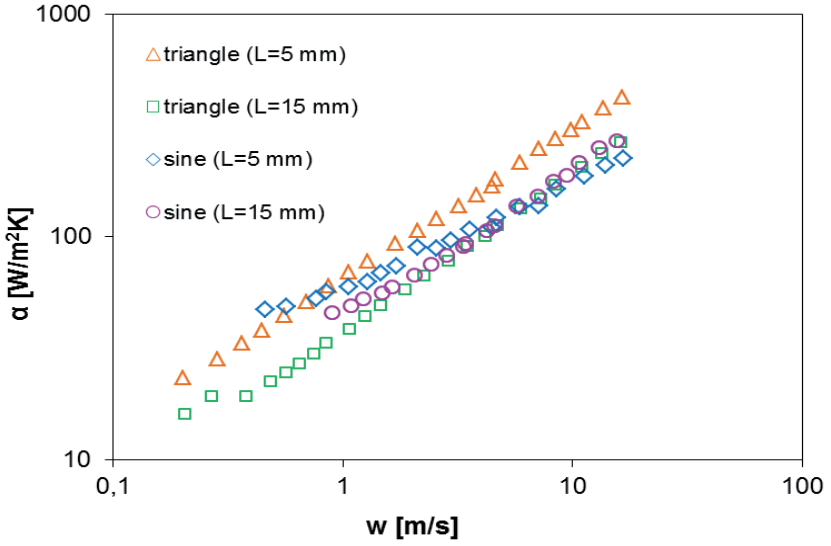

Fig. 8. Comparison of the heat transfer coefficient (averaged over all surface area of the channel walls) for different channels

Rys. 8. Porównanie współczynnika wnikania ciepła (uśrednionych na całej powierzchni ścian kanału) dla różnych kanałów

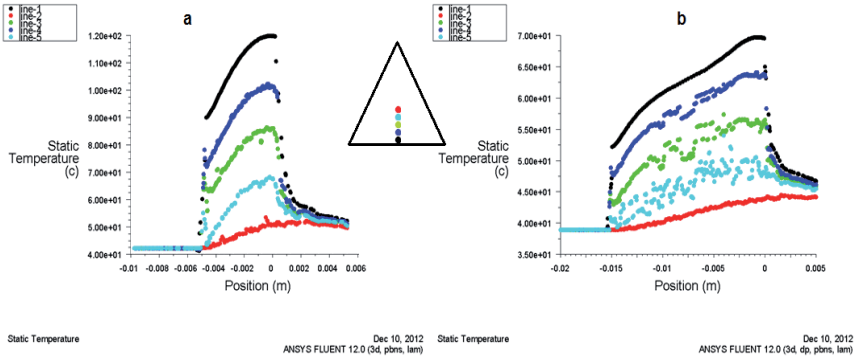

Fig. 9. Temperature distribution in different places of air stream cross-section in triangular channel: a – L=5 mm; w=16.231 m·s^{-1}; $\dot{q}$ =24503.57 W·m^{-2}; b – L=15 mm; w=16.507 m·s^{-1}; $\dot{q}$ =7058.218 W·m^{-2}

Rys. 9. Rozkład temperatur w różnych miejscach przekroju poprzecznego strumienia powietrza dla kanału trójkątnego: a – L=5 mm; w=16.231 m·s^{-1}; $\dot{q}$ =24503.57 W·m^{-2}; b – L=15 mm; w=16.507 m·s^{-1}; $\dot{q}$ =7058.218 W·m^{-2}

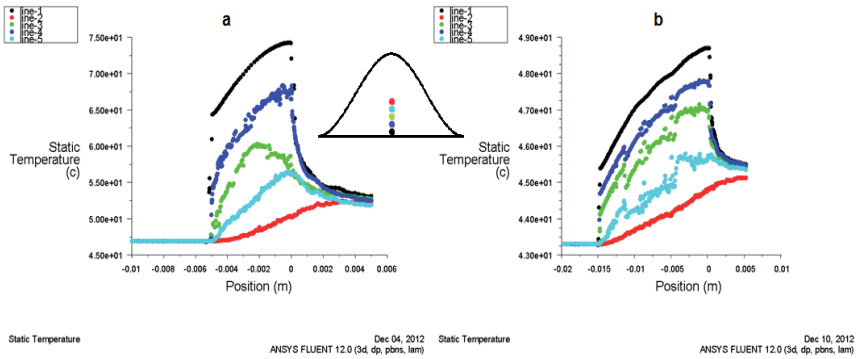

Fig. 10. Temperature distribution in different places of air stream cross-section in sinusoidal channel: a – L=5 mm; w=16.595 m·s^{-1}; $\dot{q}$ =9466.676 W·m^{-2}; b – L=15 mm; w=15.604 m·s^{-1}; $\dot{q}$ =1116.378 W·m^{-2}

Rys. 10. Rozkład temperatur w różnych miejscach przekroju poprzecznego strumienia powietrza dla kanału sinusoidalnego: a – L=5 mm; w=16.595 m·s^{-1}; $\dot{q}$ =9466.676 W·m^{-2}; b – L=15 mm; w=15.604 m·s^{-1}; $\dot{q}$ =1116.378 W·m^{-2}

3.2. FLOW RESISTANCE

The pressure distribution (hypertension compared to atmospheric pressure) in different cross-sectional areas (labeled control sections P1 – P4) is presented in Fig. 11 – 14. Sections P3 - P4 correspond to the physical channel structure under the test. In this section, the channel wall is shown as thick black line.

It is shown before entering the channel (section labeled P1) that the thickness of the channel walls has an effect on the pressure, which is higher at this point. At the channel inlet (P3), at the channel outlet (P4) and behind the channel (P2) the pressure is higher in the core and structures curvatures, while in the wall region the pressure is lower. Behind the channel, on the surface corresponding to the thickness of the wall, the pressure can reach small negative values. Segment P3 – P4 corresponds to the channel, therefore, the differential pressure should take into account only the viscous friction in the channel in laminar flow. However, the pressure difference between P1 – P2 includes an additional pressure drop due to the drag forces induced by the channel walls.

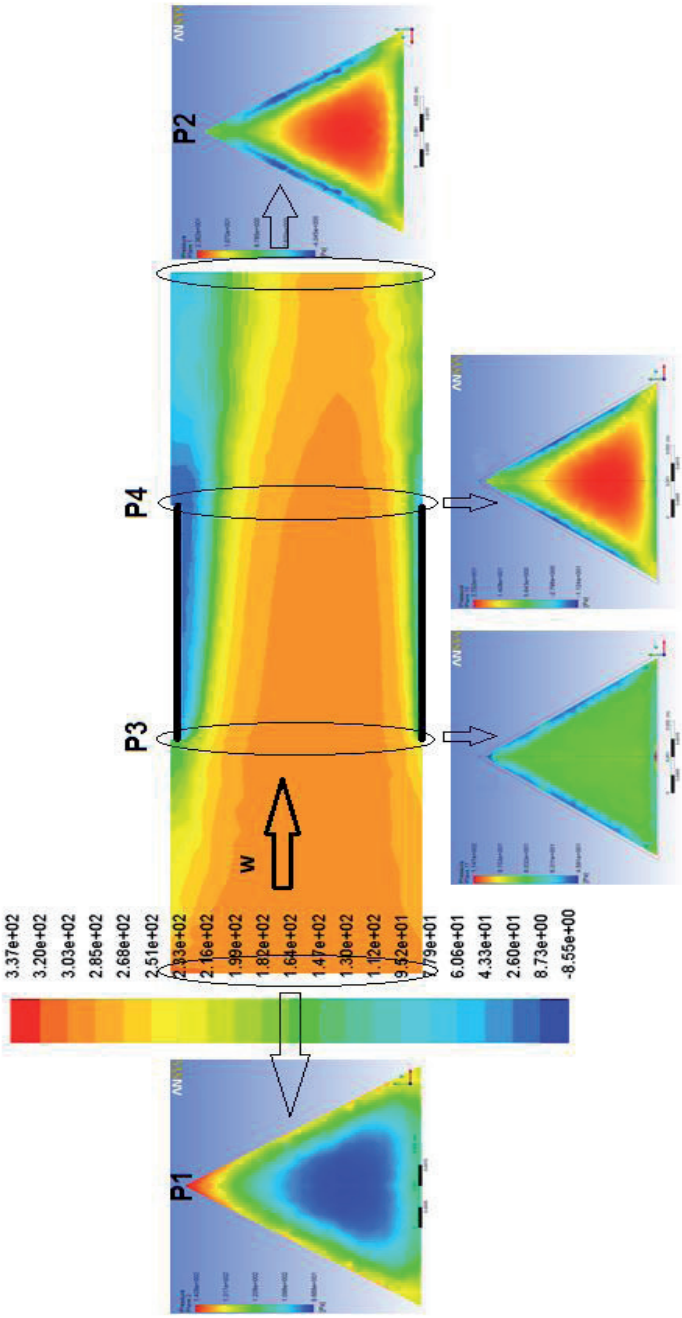

Fig. 11. Pressure distribution in air stream in triangular channel (L=5 mm; w=18.469 m·s^{-1}; t=66°C; Re=2843.355). Caution: pressure scales for cross-sections, marked as P1 – P4, are different from the main picture

Rys. 11. Rozkład ciśnień w strumieniu powietrza dla kanału trójkątnego (L=5 mm; w=18.469 m·s^{-1}; t=66°C; Re=2843.355). Uwaga: skale ciśnienia dla przekrojów poprzecznych, oznaczonych jako P1 – P4, są różne niż dla głównego rysunku

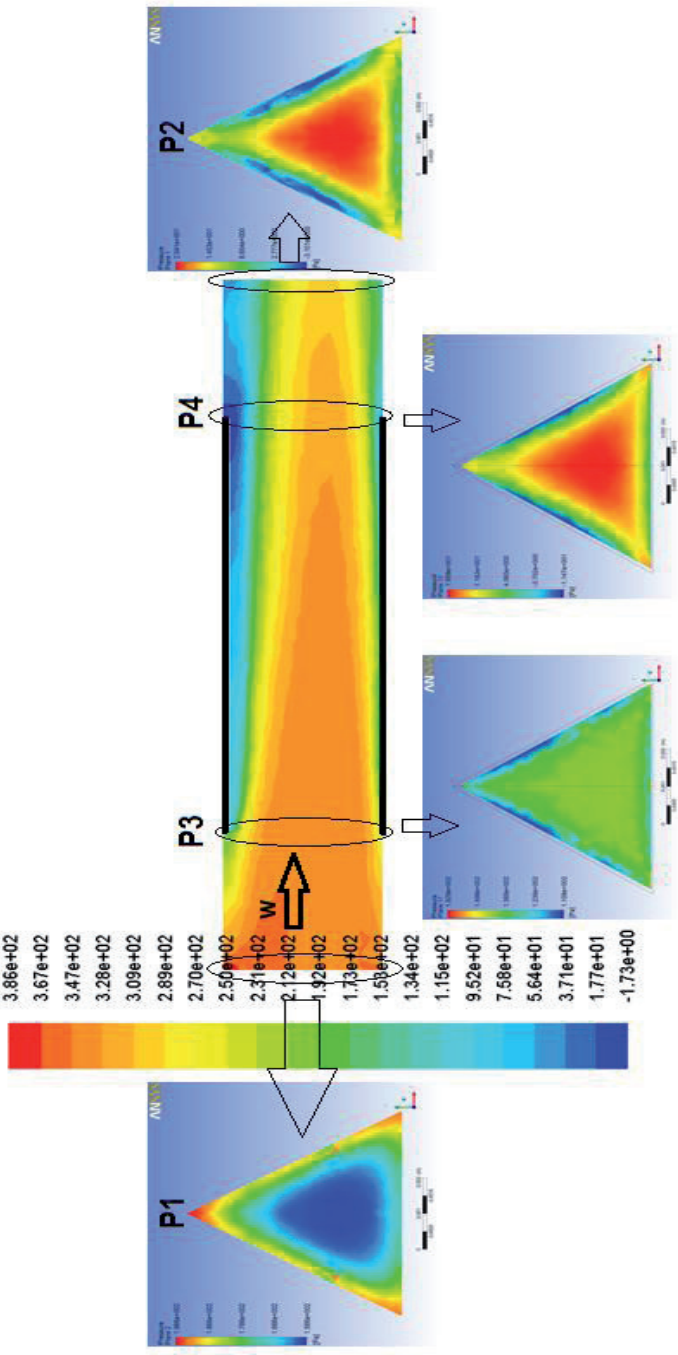

Fig. 12. Pressure distribution in air stream in triangular channel (L=15 mm; w=18.268 m·s^{-1}; t=58.2 °C; Re=2878.174). Caution: pressure scales for cross-sections, marked as P1 – P4, are different from the main picture

Rys. 12. Rozkład ciśnień w strumieniu powietrza dla kanału trójkątnego (L=15 mm; w=18.268 m·s^{-1}; t=58.2 °C; Re=2878.174). Uwaga: skale ciśnienia dla przekrojów poprzecznych, oznaczonych jako P1 – P4, są różne niż dla głównego rysunku

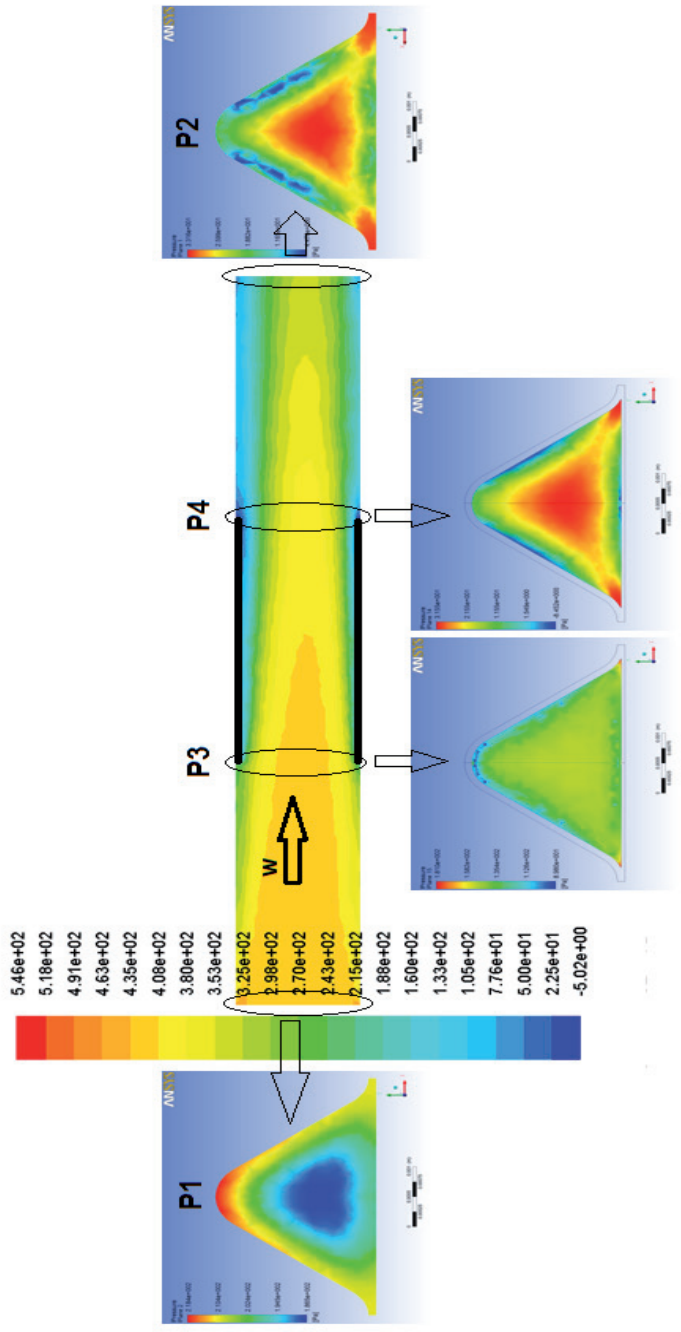

Fig. 13. Pressure distribution in air stream in sinusoidal channel (L=5 mm; w=19.359 m·s^{-1}; t=76.7 °C; Re=1538.378). Caution: pressure scales for cross-sections, marked as P1 – P4, are different from the main picture

Rys. 13. Rozkład ciśnień w strumieniu powietrza dla kanału sinusoidalnego (L=5 mm; w=19.359 m·s^{-1}; t=76.7 °C; Re=1538.378). Uwaga: skale ciśnienia dla przekrojów poprzecznych, oznaczonych jako P1 – P4, są różne niż dla głównego rysunku

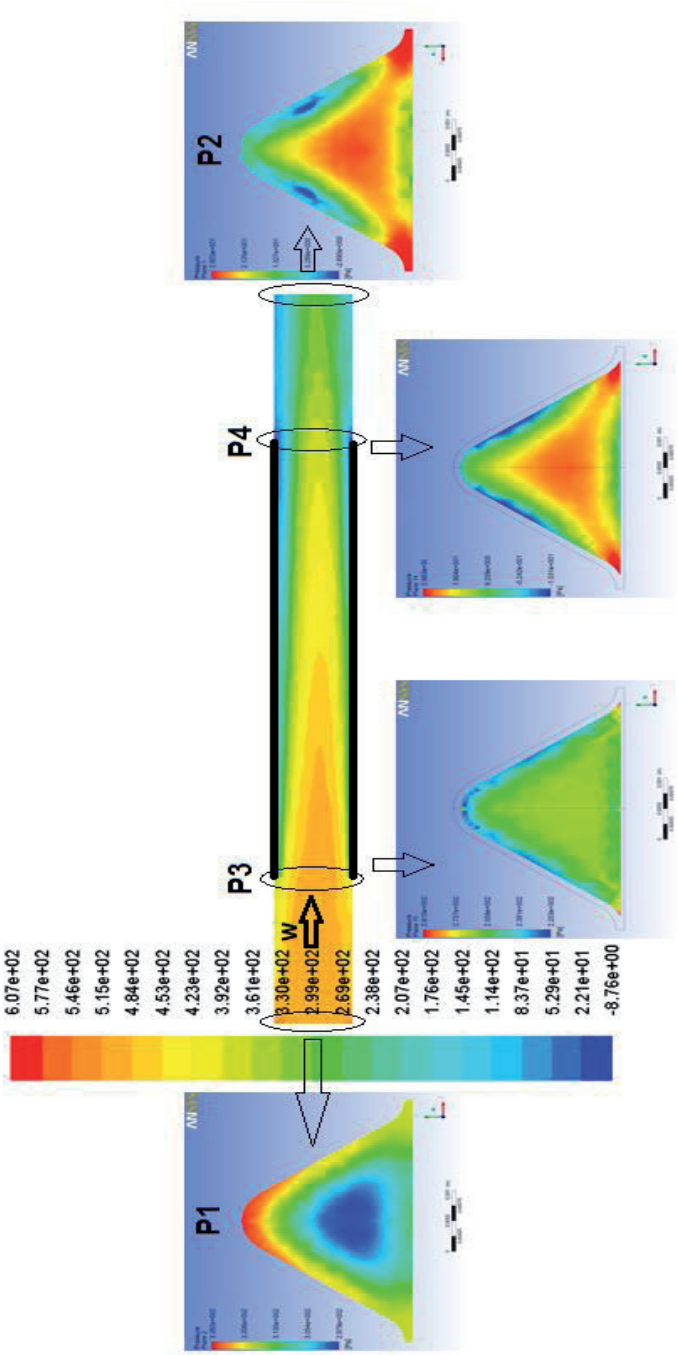

Fig. 14. Pressure distribution in air stream in sinusoidal channel (L=15 mm; w=18.931 m·s^{-1}; t=80.7 °C; Re=1477.616). Caution: pressure scales for cross-sections, marked as P1 – P4, are different from the main picture

Rys. 14. Rozkład ciśnień w strumieniu powietrza dla kanału sinusoidalnego (L=15 mm; w=18.931 m·s^{-1}; t=80.7 °C; Re=1477.616). Uwaga: skale ciśnienia dla przekrojów poprzecznych, oznaczonych jako P1 – P4, są różne niż dla głównego rysunku

Comparison of the pressure distribution in the air stream, shown in Fig. 11 – 14, indicates that the pressure value is not only the wall thickness result, but also the channel length and shape. The pressures are higher in the case of sinusoidal structures (especially in the corners) and for longer channels.

In order to calculate the pressure drop, thus the Fanning factor, the average value of pressure at channel inlet (marked as P1 and P3 in Fig. 11 – 14) and channel outlet (marked as P2 and P4 in Fig. 11 – 14) was calculated. Segment P3 – P4 corresponds to the channel, therefore, Fanning factor should take into account only the viscous resistance (skin friction) in the channel in laminar flow. However, the pressure difference P1 – P2 includes an additional pressure drop due to the drag forces, which results from the channel wall thickness.

The pressure drop as a function of fluid velocity for different channels is presented in Fig. 15. It is shown that the pressure drop for different channels is similar, but for the triangular channels it is slightly lower than for sine channels.

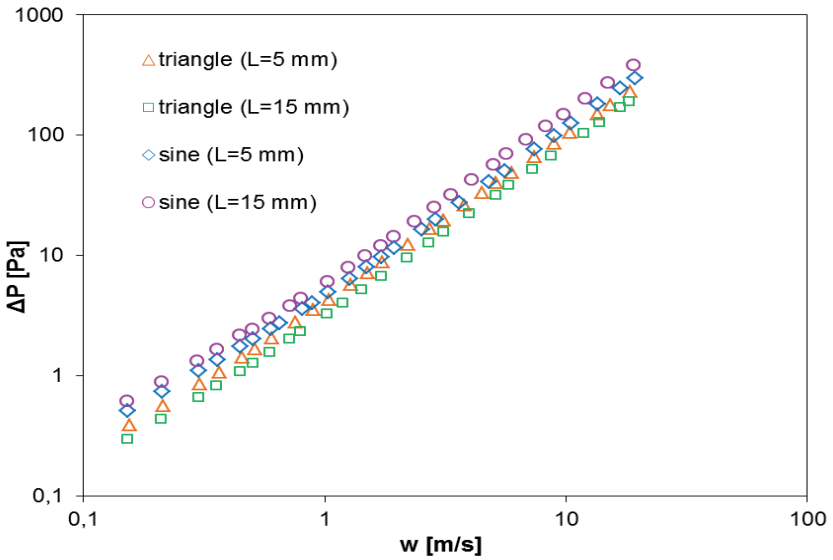

Fig. 15. Comparison of the pressure drop coefficient for different channels
Rys. 15. Porównanie spadku ciśnienia dla różnych kanałów

4. CONCLUSSIONS

The paper analyses the heat transfer and flow resistance for different cross-sectional shapes, and lengths, of short capillary channels in the conditions of a de-

veloping laminar flow. The analysis was performed using CFD technique. The temperature and pressure distribution was taken into account to decide, which channel is more effective. The comparison of heat transfer coefficients for channels has shown that the shorter the channel length, the more intense the heat transfer. The flow resistance of longer channels is somewhat higher when comparing to the shorter ones.

Both the flow resistance and heat transfer intensity are comparable for the studied channels. However, both of them can be easily regulated by simple change of the channel length. This opens door to the optimization of the reactor transfer and friction properties, according to the requirements of the reaction kinetics.

FLUENT CFD software allows to perform preliminary studies of heat transfer and flow resistance before the experimental ones. Numerical modeling should be a first step to see the initial results and thus to improve first assumptions.

SYMBOLS – OZNACZENIA

A_c -channel cross-sectional area, m^2
przekrój poprzeczny kanału
c_p -specific heat, $J \cdot kg^{-1} \cdot K^{-1}$
ciepło właściwe
L -heated channel length, m
długość kanału ogrzewanego
M_w -molecular weight, $kg \cdot mol^{-1}$
masa molowa
P -pressure, Pa
ciśnienie
p_{op} -operating pressure, Pa
ciśnienie pracy
q -heat flux, $W \cdot m^{-2}$
strumień cieplny
R -universal gas constant, $J \cdot mol^{-1} \cdot K^{-1}$
uniwersalna stała gazowa
Re -Reynolds number, $Re=w \cdot D_h \cdot \rho \cdot \eta^{-1}$
liczba Reynoldsa
T -temperature, K
temperatura
T_m -mixing cup temperature, K
temperatura wymieszania
t -temperature, ˚C
temperatura
w -fluid axial velocity, $m \cdot s^{-1}$
prędkość osiowa płynu
w_m -fluid mean axial velocity, $m \cdot s^{-1}$
prędkość osiowa płynu
x -coordinate
współrzędna

η -dynamic viscosity, Pa·s
dynamiczny współczynnik lepkości
λ -thermal conductivity, $W \cdot m^{-1} \cdot K^{-1}$
współczynnik przewodzenia ciepła
ρ -density, kg m^{-3}
gęstość

REFERENCES – PIŚMIENNICTWO CYTOWANE

[1] PRESTI M., PACE L., HODGSON J., BELLA G., DE MAIO A., *A Computational and Experimental Analysis for Optimization of Cell Shape in High Performance Catalytic Converters*. Society of Automotive Engineers (SAE) Paper 2002-01-0355.
[2] Joshi S. Y., Harold M. P., Balakotaiah V., *Overall mass transfer coefficients and controlling regimes in catalytic monoliths*. Chem. Eng. Sc. 2010, 65, 1729.
[3] Gundlapally S. R., Balakotaiah V., *Heat and mass transfer correlations and bifurcation analysis of catalytic monoliths with developing flows.* Chem. Eng. Sc. 2011, 66, 1879.
[4] SHAH R.K., LONDON A.L., *Laminar Flow Forced Convection in Ducts.* Academic Press, New York, 1978.
[5] JAWORSKI Z., *Numeryczna mechanika płynów w inżynierii chemicznej i procesowej.* Akademicka Oficyna Wydawnicza EXIT, Warszawa, 2005.
[6] KMIOTEK M., *Przegląd solverów numerycznych stosowanych w mechanice obliczeniowej.* Wydział Rzeszow University of Technology, Faculty of Mechanical Engineering and Aeronautics, Scientific Bulletin of Chełm, Section of Mathematics and Computer Science, No. 1/2008, available in Internet: <http://www.pwszchelm.pl/kis/publikacje/VII/Kmiotek.pdf>.

MARZENA IWANISZYN, JOANNA ŁOJEWSKA, ANDRZEJ KOŁODZIEJ

MODELOWANIE NUMERYCZNE WYMIANY CIEPŁA I OPORÓW PRZEPŁYWU W KRÓTKICH KANAŁACH: SZCZEGÓŁOWY OPIS

Dopalanie katalityczne stosowane jest w celu ograniczenia emisji spalin samochodowych, metanu i lotnych związków organicznych do atmosfery. Proces ten realizowany jest w reaktorach z wypełnieniem monolitycznym posiadającym kilkadziesiąt równoległych kanałów o różnym kształcie przekroju poprzecznego. Najczęściej struktura monolityczna posiada kanały kwadratowe. Prezentowana praca poświęcona jest rzadziej spotykanym kanałom trójkątnym i sinusoidalnym.

Najważniejszym elementem dopalania katalitycznego jest intensyfikacja procesu transportu ciepła i masy. W pracy [2] udowodniono, że skrócenie długości kanału umożliwi uzyskanie znacznie większych współczynników wnikania ciepła i masy. Dlatego obliczenia numeryczne przeprowadzono dla długości kanałów 5 i 15 mm w celu dokonania porównania zarówno wpływu kształtu, jak i długości kanału na rozkład temperatur i ciśnień w przekroju poprzecznym strumienia powietrza.

Symulacje komputerowe (CFD) wymiany ciepła i oporów przepływu wykonano w programie ANSYS FLUENT. Przygotowano trójwymiarowe geometrie pojedynczych kanałów, wygenerowano siatki obliczeniowe, wprowadzono parametry stosowanych materiałów, ustalono równania ciągłości, pędu i ciepła oraz warunki początkowe i brzegowe.

Graficznie rozkłady temperatur i ciśnień w krótkich kanałach trójkątnych i sinusoidalnych przedstawiono dla największych badanych prędkości przepływu. Umieszczono także wykresy prezentujące rozkład temperatur w różnych miejscach przekroju poprzecznego strumienia powietrza.

Symulacje wykazały, że gradient temperatur jest największy na ściance (odcinek środkowy), a temperatura strumienia powietrza jest najwyższa w wierzchołkach (zakrzywieniach) struktur. Ponadto w kanale sinusoidalnym strumień powietrza ogrzewa się do wyższej temperatury, co jest rezultatem w przybliżeniu dwukrotnie większej powierzchni geometrycznej struktur sinusoidalnych w porównaniu ze strukturami trójkątnymi. Wpływ na wymianę ciepła ma także długość kanału. W wyniku przepływu powietrza przez dłuższy kanał osiągane są wyższe temperatury. Jednak intensywność wnikania ciepła jest większa w kanale krótszym. Aby doszło do całkowitego wyrównania temperatur w przekroju poprzecznym, niezbędne jest pokonanie przez płynący strumień powietrza znacznej odległości za wylotem z kanału z uwagi na laminarny charakter przepływu (wspomniana wirtualna, nie ogrzewana ściana kanału za jego fizycznym wylotem). Przed wlotem do kanału grubość ścianki kanału ma wpływ na wartość ciśnienia, które w tym miejscu jest większe. Na wlocie do kanału, na wylocie z kanału i za wylotem, w rdzeniu i zakrzywieniach struktur ciśnienie jest większe, natomiast w obszarze przyściennym ciśnienie jest mniejsze. Ponadto wpływ na wartość ciśnienia ma nie tylko grubość ścianki kanału, ale także długość kanału i jego kształt. Wartości ciśnienia są większe w przypadku struktur sinusoidalnych (zwłaszcza w narożach) i dla dłuższych kanałów.